

Article citation info:

Błażej R, Jurdziak L, Kirjanów-Błażej A, Rzeszowska A, Kostrzewa P, Improving the effectiveness of the DiagBelt+ diagnostic system - analysis of the impact of measurement parameters on the quality of signals, *Eksploracja i Niezawodność – Maintenance and Reliability* 2024; 26(3) <http://doi.org/10.17531/ein/187275>

Improving the effectiveness of the DiagBelt+ diagnostic system - analysis of the impact of measurement parameters on the quality of signals

Indexed by:



Ryszard Błażej^a, Leszek Jurdziak^a, Agata Kirjanów-Błażej^{a,*}, Aleksandra Rzeszowska^a, Paweł Kostrzewa^b

^a Wrocław University of Science and Technology, Poland

^b BESTGUM Polska, Poland

Highlights

- The DiagBelt+ system contributes to increasing the reliability and safety of belt conveyors.
- The analysis of data will allow to identify the location of the most worn out place.
- Answer the question in which section the potential damage to the cover of the conveyor belt is located.

Abstract

The key issue for ensuring economic efficiency and continuous operation of conveyor transport is the recognition of the condition of the belt core. Faults in steel cords in the core are not visible during routine visual inspections, but they can be identified using magnetic diagnostic systems such as DiagBelt+. The article presents an analysis of the impact of the sensitivity threshold of the DiagBelt+ system, the diameter of cords in the core, and the belt speed on the quality of signals representing known damage: cutting of cords, their absence, and a reduction in the cross-section of the cord. The study focuses on defects to cords across the belt, as they can weaken the belt's strength and lead to a complete belt failure. The proposed results and analyses contribute to the improvement of the methodology for magnetic examination of the core's condition and the developed diagnostic system DiagBelt+. Consequently, this enhances the reliability and safety of belt conveyors in various industries, including brown coal mines where it has been implemented (PGE GiEK SA KWB O/Bełchatów), as well as in hard coal, limestone, and copper ore mines where it is used to assess the condition of belts with steel cords.

Keywords

NDT-testing, conveyor belt, DiagBelt system, magnetic method, accuracy

This is an open access article under the CC BY license (<https://creativecommons.org/licenses/by/4.0/>)

1. Introduction

Contemporary industrial processes, dominated by continuous material transport, utilize conveyor belts as an integral component for the efficient movement of raw materials and products. A crucial aspect in maintaining the reliability and safety of these conveyors is effective diagnostics of the conveyor belt's condition, which constitutes the most expensive and damage-sensitive component of the conveyor system. This

article presents research results on improving the DiagBelt+ diagnostic system, a magnetic Non-Destructive Testing (NDT) tool used to monitor the condition of conveyor belt cores. The effectiveness of the measurement system involves selecting appropriate measurement parameters (such as the system sensitivity threshold) for working conditions during testing (cord diameter and belt speed) to obtain interpretable signals.

(*) Corresponding author.

E-mail addresses:

R. Błażej (ORCID: 0000-0002-8802-9865) ryszard.blazej@pwr.edu.pl, L. Jurdziak (ORCID: 0000-0003-2353-8420) leszek.jurdziak@pwr.edu.pl, A. Kirjanów-Błażej (ORCID: 0000-0002-0011-6180) agata.kirjanow-blazej@pwr.edu.pl, A. Rzeszowska (ORCID: 0000-0002-6266-2806) aleksandra.rzeszowska@pwr.edu.pl, P. Kostrzewa pawel.kostrzewa@bestgum.pl,

Non-invasive diagnostics (NDT) of conveyor belts is crucial for detecting failures, reducing costs associated with the premature replacement of belts still in good technical condition, and monitoring wear over time. This approach significantly contributes to enhancing the overall safety of conveyor belt operation. The rate of conveyor belt wear is influenced by various factors, including the conveyor's location, length, the type of transported material, belt speed, and others [1, 9, 40, 42]. According to reliability theory, the aging process of the belt increases the risk of failure. The conveyor belt, being one of the most expensive components of the conveyor system, is subjected to intense forces and impact processes from falling rock fragments, leading to core degradation and wear on covers and edges [23]. Faults in the core, accumulated at one cross-section, can result in catastrophic stoppages due to longitudinal cuts, complete belt rupture, or splices separations. Continuous fatigue processes and ubiquitous friction at various points further reduce cover thickness and the critical impact energy, beyond which core damage occurs. Each section and segment of the belt undergoes a cyclic process of destruction as it passes under loading points and chutes.

Belt segments and connections in a loop form a series system from the perspective of reliability theory. Damage to any element of this system results in failure and downtime for all conveyors in the entire sequence. Consequently, critical conveyors are often reserved to prevent failures from causing downtime and production losses [8]. Approaches related to belt diagnostics and predictive replacements based on diagnosed conditions of sections and connections for refurbishment can significantly mitigate these risks. Belt wear is unavoidable, but the process can be significantly slowed down. To achieve this, it is necessary to understand all factors influencing the rate of belt wear, such as belt parameters, chute construction [11, 12, 21, 37], parameters of the transported material [13], conveyor parameters [6], and working conditions and intensity of use, including the quantity and energy of falling rock fragments at loading points [1, 2]. The most susceptible part to failures in the conveyor system is the belt itself. Meeting high durability and strength standards is associated with higher production costs and prices. Belt diagnostics, enabling the quick detection of potential failures, makes economic sense because conveyor failure generates significant costs related not only to repairs but

also to downtime in the transport system and production losses [7]. In recent years, many systems have been developed to prevent catastrophic consequences of unexpected failures [17, 30, 32], as well as to assess the technical condition of conveyor belts and their degree of wear [18].

Conveyor belts can have a textile core, characterized by lower resistance to damage, and a core with steel cords, offering higher durability (Figure 1) and significantly higher performance over longer distances. The St belt core plays a crucial role, carrying loads and ensuring the exceptional strength of the entire belt. Therefore, diagnosing the core's condition is essential for the early detection of potential damage, enabling effective prevention and extending the belt's durability.

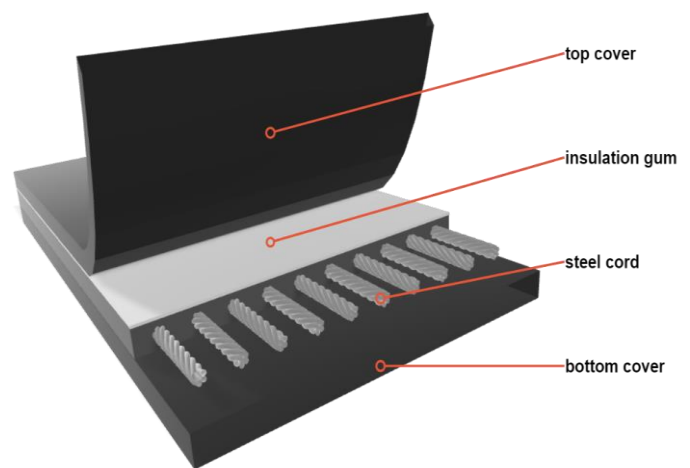


Figure 1. Conveyor belt with steel cords - construction diagram.

Non-Destructive Testing is a crucial diagnostic tool that allows the assessment of conveyor belt conditions without compromising their structure [4, 15, 36]. In the era of Industry 4.0, various diagnostic systems, such as sensors collecting real-time data, enable the monitoring of changes in the belt's condition and responsive action to potential threats can be implemented [14, 28, 43]. Periodic diagnostics allow for the examination of the belt periodically, assessing its condition and the cumulative changes, such as an increase in core failures or wear on covers. Although installing diagnostic devices on each conveyor can be costly, it contributes to safeguarding the system against catastrophic failures, and cyclic diagnostics help optimize investment costs. Such an approach is effective for both assessing the current state and identifying accumulating changes in the long-term perspective.

Available on the market, diagnostic devices for assessing the

technical condition of conveyor belt steel cores utilize various research methods. Existing systems employing X-ray radiation [16, 25] provide precise radiographic images of the cords in the belt core, but analyzing the obtained results and reviewing hundreds of images poses a significant challenge. Moreover, the use of systems employing X-ray radiation requires specific safety measures to avoid exposing operators to radiation. Vision systems (e.g., [19, 38]) are not applicable in conditions of high dust levels, commonly found in mines. Furthermore, they only allow monitoring the technical condition of the belt covers, without enabling the assessment of the state of the cords in the belt core. Devices utilizing magnetic properties are also available, both for diagnosing belt cords and for diagnosing steel wire ropes [27, 34, 35]. The device [41], operating similarly to the DiagBelt+ system analyzed in the article, aggregates the obtained signal from a 40 cm width of the belt into a single measurement channel, thereby preventing the identification of individual failures. The research described in the article showcases the magnetic system DiagBelt+, its application for measurements under various parameters, and the obtained measurement results. The goal of the conducted and described research was to enhance the efficiency of the diagnostic system and determine the impact of measurement parameters on the magnitude of the obtained measurement signal. The principle of operation and signal processing within the measuring strip has been described in [3–5].

2. DIAGBELT+ DIAGNOSTIC SYSTEM

The DiagBelt+ system operates by monitoring the magnetic properties of the conveyor belt with steel cords. Permanent magnet heads are placed above and below the examined belt section at equal distances from it, typically around 35 mm, allowing for the magnetization of the cords in the core. The measuring head, consisting of inductive coils, measures the magnetic field strength (magnetic induction) generated by the magnetized belt core. In the event of failures such as cracks, cuts, missing cords, or a reduction in cross-sectional area, the magnetic field undergoes changes, which are detected by the measuring head. These changes are then used to identify failures, determine their size, and ascertain their type.

The measuring head consists of 90 coils spaced at equal

intervals of 25 mm, arranged in a single line along a length of 2250 mm within the working space. Measurement signals from these inductive coils are amplified, collected in the data acquisition module, and further processed. The head is mounted at a specific distance from the belt, adjusted to the belt speed and the diameter of the cords in the core. The distance is one of the parameters influencing the magnitude of the obtained signal. The signals collected by the head undergo thresholding, as per equation (1), and are recorded in the form of matrices of discrete values of -1, 0, and +1. This facilitates data analysis. The software also allows for data storage and export in .csv file format.

$$y = \begin{cases} -1, & x \leq th_{min} \\ 0, & x \in (th_{min}, th_{max}) \\ 1, & x \geq th_{max} \end{cases} \quad (1)$$

where:

x – original value before thresholding,

y – value after thresholding,

th_{min} – minimum detection threshold based on the adopted system sensitivity threshold,

th_{max} – maximum detection threshold based on the adopted system sensitivity threshold,

During measurements, magnetizing heads are installed both above and below the belt at equal distances from the belt covers, typically optimized to be 30-40 mm. To detect discontinuities in the cords or the loss of their metallic cross-section, steel cords must be magnetized beforehand. The magnetizing strips conduct several cycles of the belt's circuit (approximately 6-8 for the initial scan and 2-3 for subsequent scans after a specific period, e.g., several months. The decision regarding the number of magnetization loops performed is made individually each time by comparing the signal obtained from the last two loops. For a fully magnetized belt, the signal remains unchanged. During the actual measurements, permanent magnet strips remain installed on the conveyor.). Figure 2 illustrates the arrangement of the permanent magnet heads and the measuring head.

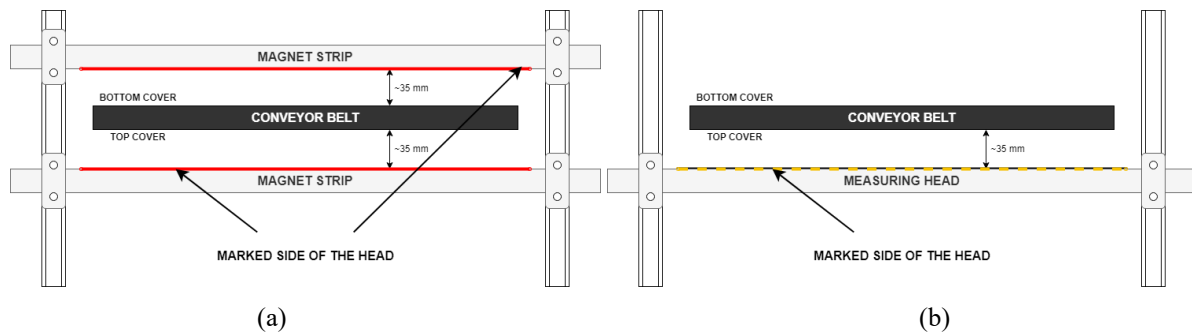


Figure 2. Installation diagram of magnet heads (a) and measuring head (b).

Additionally, the system includes a tachometer for real-time monitoring of the belt speed and the location of detected signals along its length.

An example of signals obtained after examining one of the conveyor belts operating in industrial conditions (in one of the brown coal mines, overburden transport, velocity approximately 6 m/s, belt loop length approximately 1900 m, belt width 2.25 m, section length approximately 235 m, belt after 2nd refurbishment, lifetime 7 months (15% of predicted lifetime)) is presented in Figure 3. The signal across the full width of the belt represents a belt splice. Despite its relatively young age of 7 months, this conveyor belt shows a significant number of failures. This is a result of the actual operating time of the core being much longer, as the belt has already undergone

refurbishment twice. In a 235-meter section, 808 failures have been recorded, averaging 3.44 failures per linear meter of the belt. This damage density already exceeds the accepted threshold in the mine (3.2 failures/m), beyond which a new belt is so damaged that it cannot be refurbished again. The number of failures on the belt suggests that perhaps not all significant failures were repaired during refurbishment, or there may be another factor causing such a rapid rate of new failures. Conducting a scan immediately after the installation of the section (rather than after 7 months of regular operation) would allow for an assessment of the effectiveness of the refurbishment process. However, considering that the belt has already undergone refurbishment twice, it will continue to operate until it is decommissioned for scrapping.

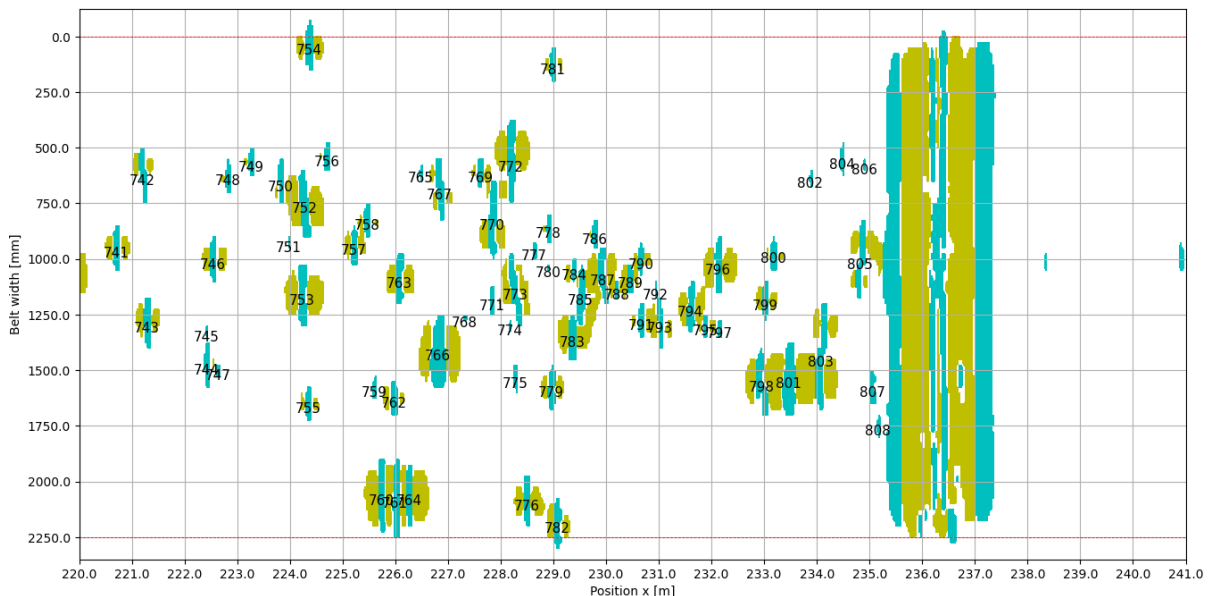


Figure 3. Example of a recorded signal.

The magnitude of damage signals varies depending on the size of the damage, the distance of the measuring head from the conveyor belt (g), the belt speed (v), and the established

sensitivity threshold (s). Long-term practice in assessing the technical condition of the conveyor belt core using the magnetic method has allowed for the adjustment of appropriate

measurement parameters, such as the distance of the measuring head from the belt surface and sensitivity, to the characteristics of a given belt (operating at a specific speed, with a specified diameter of the cords, and a specified distance between the cords) [31]. Thanks to precise adjustments of measurement parameters, it is possible to identify cord damage even in the case of belts with different nominal strengths and different operating speeds. Minor damage, such as partial cord damage, generates a damage signal concentrated on only a few measurement channels (2-3). As the size and complexity of the damage increase, the field of the recorded change in the magnetic field also increases, and two accompanying clouds of points with opposite polarizations of the magnetic field change appear. This means that small failures generate small signals (marked in the images as a blue cloud of points), while more extensive failures are characterized by the coexistence of two adjacent clouds (marked in yellow). It is worth noting that the location of the damage is unambiguously determined by the cloud of points located in the center of the damage signal (marked in blue), even if the signal consists of three clouds of points.

As part of the project POIR.01.01.01-00-1194/19 funded by the National Center for Research and Development, comprehensive studies were conducted at various stages aimed at developing and implementing the DiagBelt+ diagnostic system to assess the technical condition of conveyor belts in the Belchatów lignite mine. The first step involved assessing the effectiveness of the magnetic system in detecting damage to the belt core on a test conveyor in the Laboratory of Belt Transport at Wrocław University of Science and Technology (LTT). Subsequently, using a new measuring head, a comparative study of belts on conveyors in the mine was carried out. The subsequent stages included the construction of the DiagBelt+ system, involving the purchase of the measuring head and the development of software for data analysis, all while considering the operational requirements of the mine. As the project progressed, the DiagBelt+ system was tested in motion on selected conveyors in the deployment location. The final result of the project was the creation of an advanced diagnostic system enabling a precise assessment of the condition of conveyor belts, which could replace the previously used method based mainly

on visual assessment and the calendar lifespan of the belts. The implementation of the DiagBelt+ system aimed to streamline the process of directing belts for refurbishment and the refurbishment itself by eliminating the need for unnecessary repairs, resulting in more efficient use of resources and increased durability of conveyor belts. The implemented system is an integral part of activities related to monitoring and maintaining conveyor belts. The created and appropriately trained team of mine workers is responsible for examining belts working on conveyors, independently analyzing the obtained results. Decisions regarding the direction of belts for the refurbishment process are made based on the conducted analyses, where the covering is milled, and the most serious core damage is repaired. The previously used measure of assessing the technical condition of belts in the mine, based mainly on the calendar lifespan of the belt, proved to be much less effective compared to the applied DiagBelt+ system. Traditional assessment, based on visual inspection of belt covers and information about the age of the belt, often resulted in directing belts for refurbishment that were, in fact, in good technical condition and could continue to operate.

The implemented system is an integral part of activities related to monitoring and maintenance of conveyor belts. The created and properly trained team of mine workers is responsible for inspecting belts on conveyor systems, independently analyzing the obtained results. Decisions regarding directing belts to the refurbishment process, where the cover is milled, and the most serious core damage is repaired, are made based on these analyses.

The traditional measure of assessing the technical condition of belts used in the mine, primarily relying on the calendar life of the belt, proved to be significantly less effective compared to the DiagBelt+ system [22]. Relying on visual inspection of belt covers and information about the age of the belt often led to directing belts to refurbishment that were, in reality, in good technical condition and could continue to operate.

From the perspective of the mine and the belt refurbishment process, a key aspect is the identification of damage involving multiple adjacent cords (with significant transverse dimensions). Such extensive damage has a significant impact on reducing the strength of the belt in cross-section. Therefore, precise detection

of defects of this kind becomes essential. The DiagBelt+ system enables the identification and localization of areas with damage; however, classifying obtained signals remains challenging. The necessity of correctly recognizing signals generated by damage with significant transverse dimensions formed the basis for creating a model conveyor belt and analyzing the signals obtained during its testing.

3. MODEL CONVEYOR BELT

Many types of damage produce similar signals – the core cords in the conveyor belt can be crushed, cut, or corroded, and the differences in the system's magnetic signal are often minimal and imperceptible to the human eye, even for an experienced operator. The most common subject of diagnostics is a partially worn-out belt, one that will still be in use after the examination. Uncovering the core of the belt to inspect the damage to the cords and comparing them with the obtained images of the magnetic signal and their 2D digital representation for control of the visual classification by the operator is not possible. This is impractical due to the enormous surface that would need to be exposed by milling the covers to find all types of damage. Additionally, it is uncertain whether the milling process to the cords themselves would not cause new damage. A proper description and classification of types of damage to the core of the conveyor belt are essential for assessing the condition and predicting the development of damage over time. To obtain a database of signals generated by known types and sizes of

damage (known geometry), a model conveyor belt with simulated core damage was designed.

To minimize the influence of adjacent cords in the core of St-type belts, individual cords were embedded in the rubber cover of a textile belt with a length of 17,400 mm and a width of 900 mm. Such a loop can be installed on a conveyor belt in the LTT. The applied textile belt is EP 1000/4 4+2, with no visible signs of use – a four-ply belt with a polyester-polyamide core, with rubber covers nominally 4 mm thick on the carrying side and 2 mm on the rolling side. It is a flame-resistant belt designed for operation in power plants fueled by hard coal with a nominal strength of 1000 kN/m.

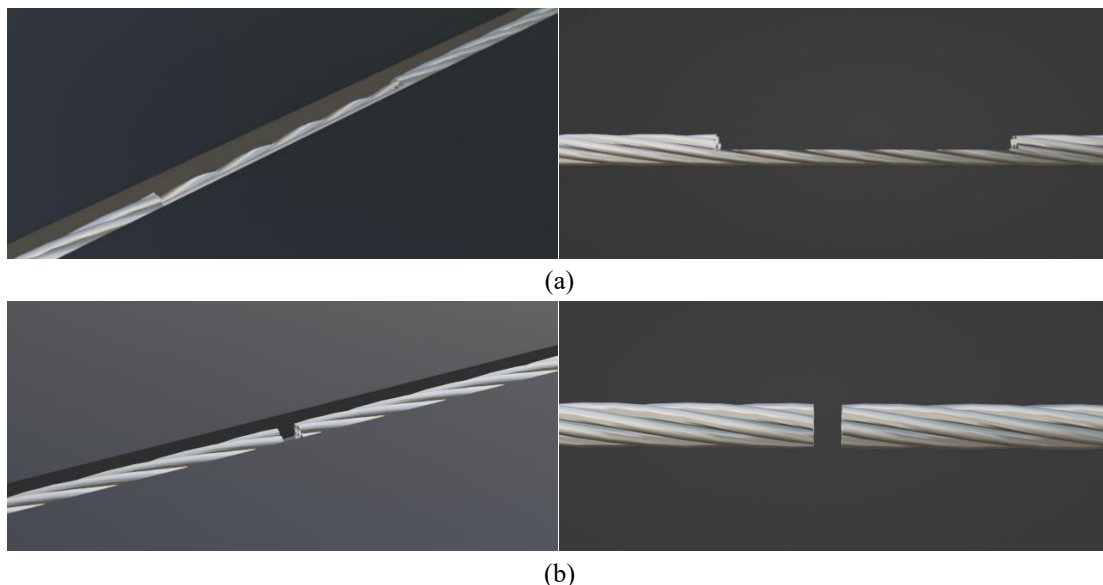
The model belt was equipped with cords that simulate common types of damage, occurring in real operating conditions of conveyor belts, significantly impacting the assessment of the technical condition of the belt core. The following types of damage were incorporated into the belt:

partial damage to a cord (U50) over a length of 2 cm (simulating corrosion),

cuts: 1 cord (U1), 2 adjacent cords (U2), 3 adjacent cords (U3),

lack of cords over a length of 2 cm: 1 cord (B1), 2 cords (B2), and 3 adjacent cords (B3).

Figure 4 presents a visualization of some types of damage – the drawings on the left side depict a cord placed in a groove made on the belt, and the drawings on the right side visualize the cords themselves.



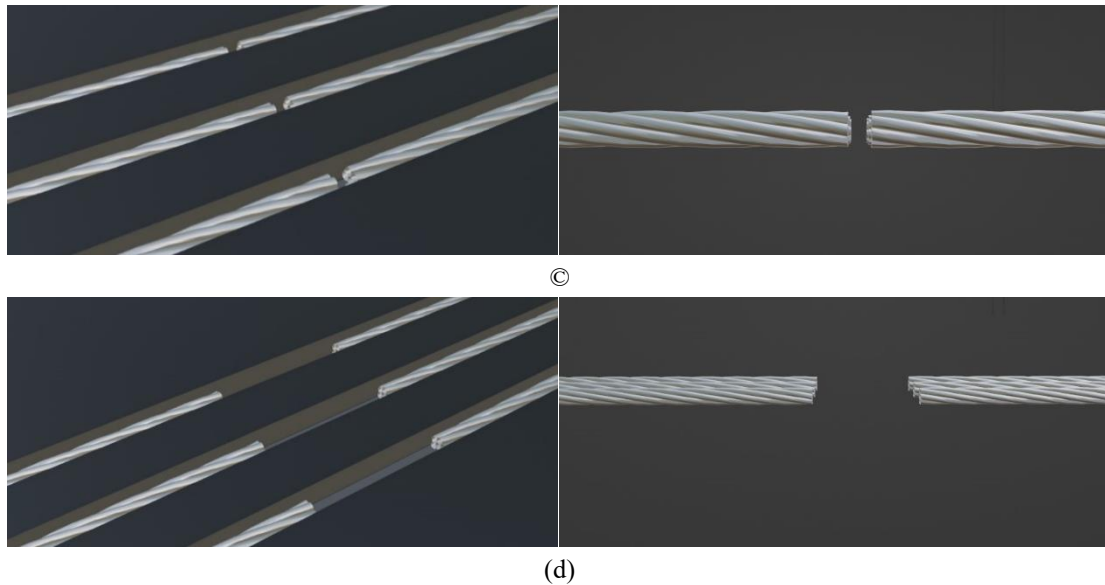


Figure 4. Visualization of model failures (a) U50 – 50% loss of a cord over a length of 20 mm (corrosion simulation), (b) U1 – cutting of 1 cord (gap 2 mm), (c) – damage to 3 adjacent cords (gap 2 mm), (d) – absence of 3 adjacent cords over a length of 2 cm.

Table 1 provides descriptions and actual dimensions of real failures. The cords were embedded in the cover rubber with a 15 mm distance between them.

Table 1. Description of model failures.

Damage symbol	Description	Damage length l [mm]	Damage width w [mm]	Damage area a [cm ²]
U50	50% damage to the cross-section of the cord (corrosion simulation)	20	15	3.0
U1	Cutting one cord	2	15	0.3
U2	Cutting two adjacent cords	2	30	0.6
U3	Cutting three adjacent cords	2	45	0.9
B1	Missing one cord over a length of 2 cm	20	15	3.0
B2	Missing two adjacent cords over a length of 2 cm	20	30	6.0
B3	Missing three adjacent cords over a length of 2 cm	20	45	9.0

In the final implementation of the designed cord, a total of 156 meters of steel cords were used, including 28 meters of cords with a diameter of $\varphi_1 = 3.0$ mm, 28 meters of cords with a diameter of $\varphi_2 = 4.0$ mm, 28 meters of cords with a diameter

of $\varphi_3 = 6.0$ mm, and 72 meters of cords with a diameter of $\varphi_4 = 7.8$ mm. A total of 90 model failures will be created on the cord, and their distribution on a single area (one cord diameter) is shown in Figure 5.

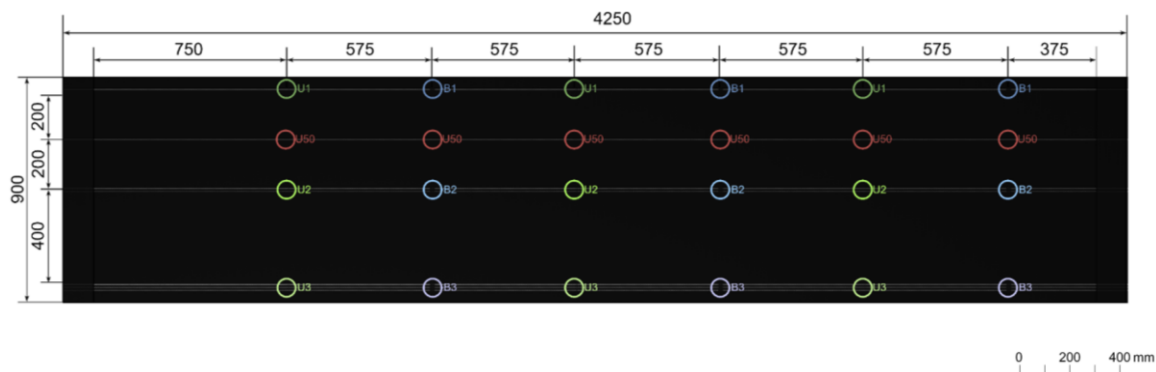


Figure 5. Projected distribution of failures on the model cord – one area.

The process of creating the model cord was divided into four stages:

Preparation of the belt – cutting the textile belt to a width of 900 mm limited by the design of the conveyor belt at the LTT.

Grooving process – creating grooves in the top cover of the textile cord, allowing for the placement of cords with different diameters and securing them appropriately.

Placement of steel cords and vulcanization – placing the cords in the previously prepared grooves. Steel cords,

positioned in dedicated areas (previously created grooves), were artificially damaged according to the modeled defects.

Splice making and installation of the belt on the Test Conveyor at LTT – creating a splice to form a loop of the model belt on the test conveyor. To facilitate the research, the cord was installed on the test conveyor at LTT.

In Figure 6, photos from the process of creating the model conveyor belt are presented.

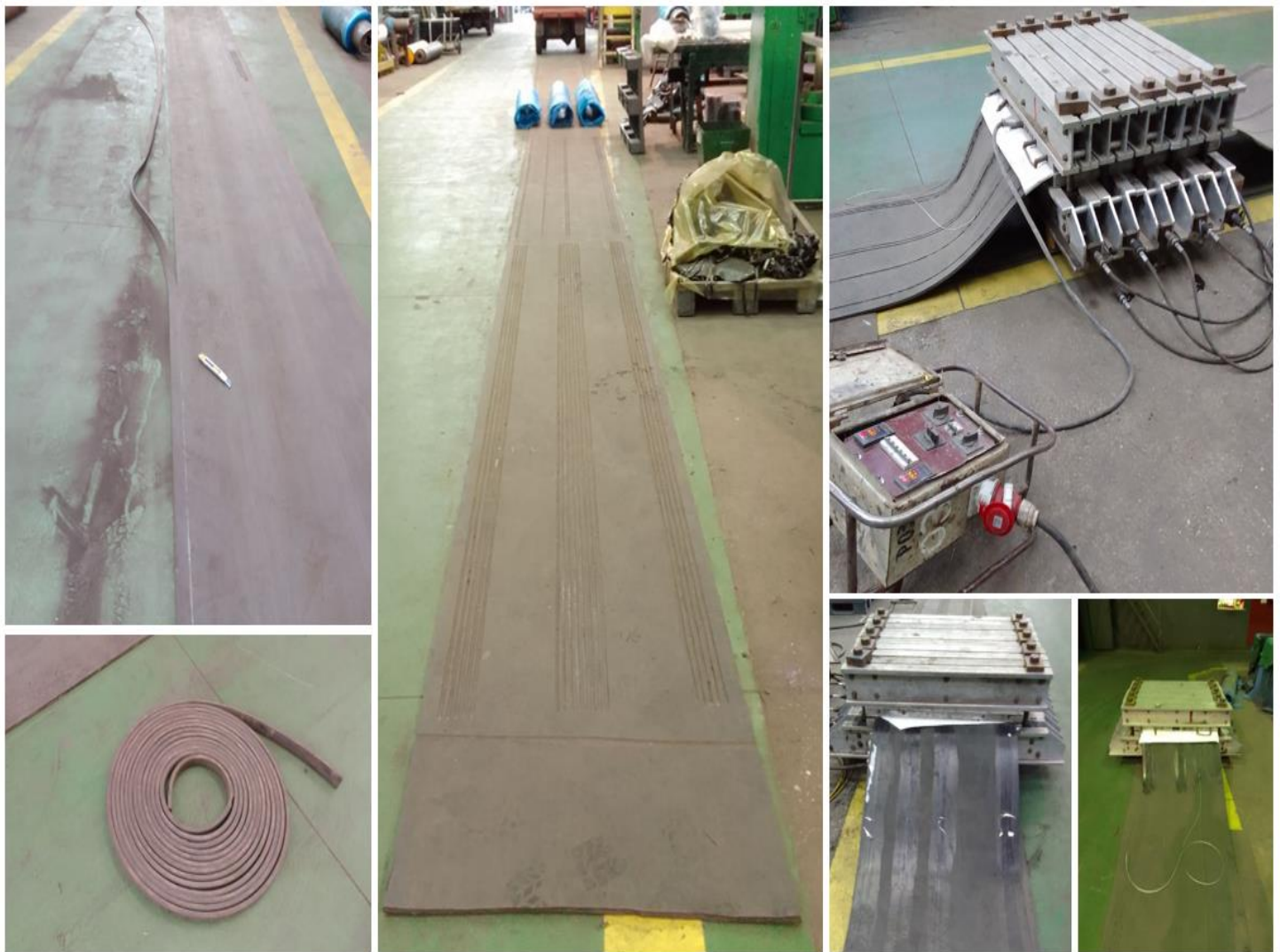


Figure 6. Photos from the stage of creating the model conveyor belt.

The belt was installed on the conveyor in the Laboratory of Belt Conveying at Wrocław University of Science and Technology.

4. RESEARCH USING THE DIAGBELT+ SYSTEM

Before conducting DiagBelt+ magnetic system tests, it is

necessary to magnetize the cords in the belt. This process requires several cycles (6-8), during which magnet heads are installed above and below the examined belt, maintaining a distance of approximately 35 mm from the covers. Figure 7 shows the installed conditioning strips using dedicated holders

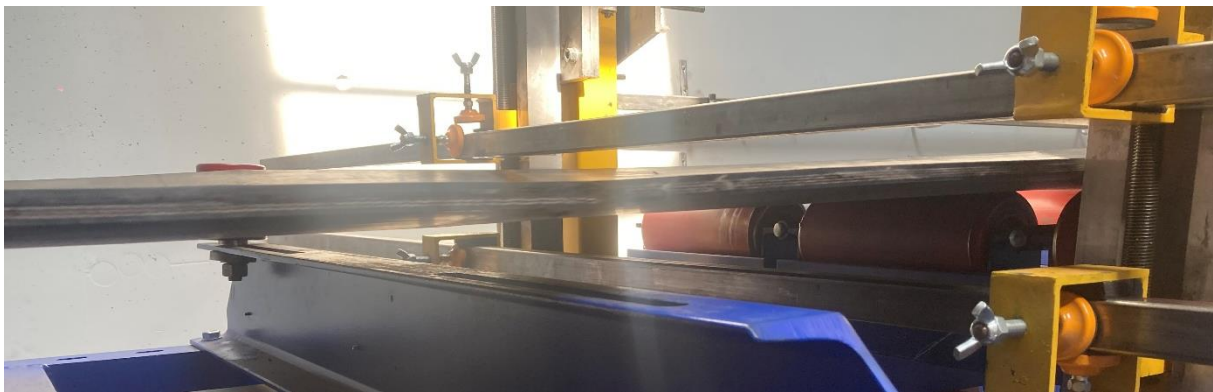


Figure 7. Installation of magnet heads above and below the examined belt.

The measuring head was mounted 30 mm from the bottom cover of the belt using special stands. Figure 8 illustrates the

installation process of the DiagBelt+ system measuring head during testing.

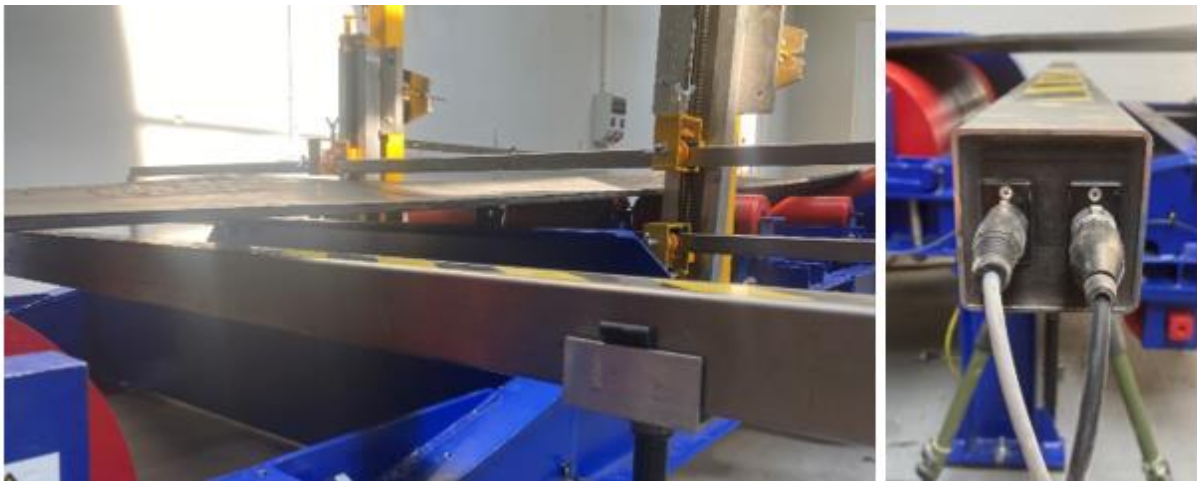


Figure 8. Installation of the DiagBelt+ system measuring head.

To measure the speed of the belt on the conveyor, and thus accurately locate the obtained signals along the length of the belt, an encoder was used. It was mounted using a "magic arm" holder. To determine the speed, it was necessary to measure the diameter of the disc to which the magnet was attached. The length of the measuring loop depends on the determined value of the belt speed. The magnet attached to the roller and rotating around its axis with each turn, changes the magnetic field, which is read by the encoder. The time between successive pulses and the diameter of the disc allow determining the linear speed of the conveyor belt, according to equation

(2).

$$v = \frac{\pi \cdot d}{t} \quad (2)$$

where:

$$v - \text{belt speed} \left[\frac{\text{m}}{\text{s}} \right],$$

d – diameter of the roller [m],

t – time between pulses [s].

The studies were conducted at three belt speeds:

$$v \in \{1.5, 2.0, 2.5\} \frac{\text{m}}{\text{s}}$$

This range of examined conveyor belt speeds is commonly encountered in hard coal mines, as well as in operations involving raw materials such as rock and ore. In open-pit mines, conveyor belt speeds can reach up to 6 m/s, and ongoing research focuses on speeds of this magnitude.

For each speed, 4 complete measuring loops were obtained at different sensitivity thresholds:

$$s \in \{2, 3, 4, 5, 6, 8, 10, 12, 14\}$$

Thus, a total of 27 measurement files were obtained. Figure 9 shows examples of three measurement loops obtained for different tested parameters.

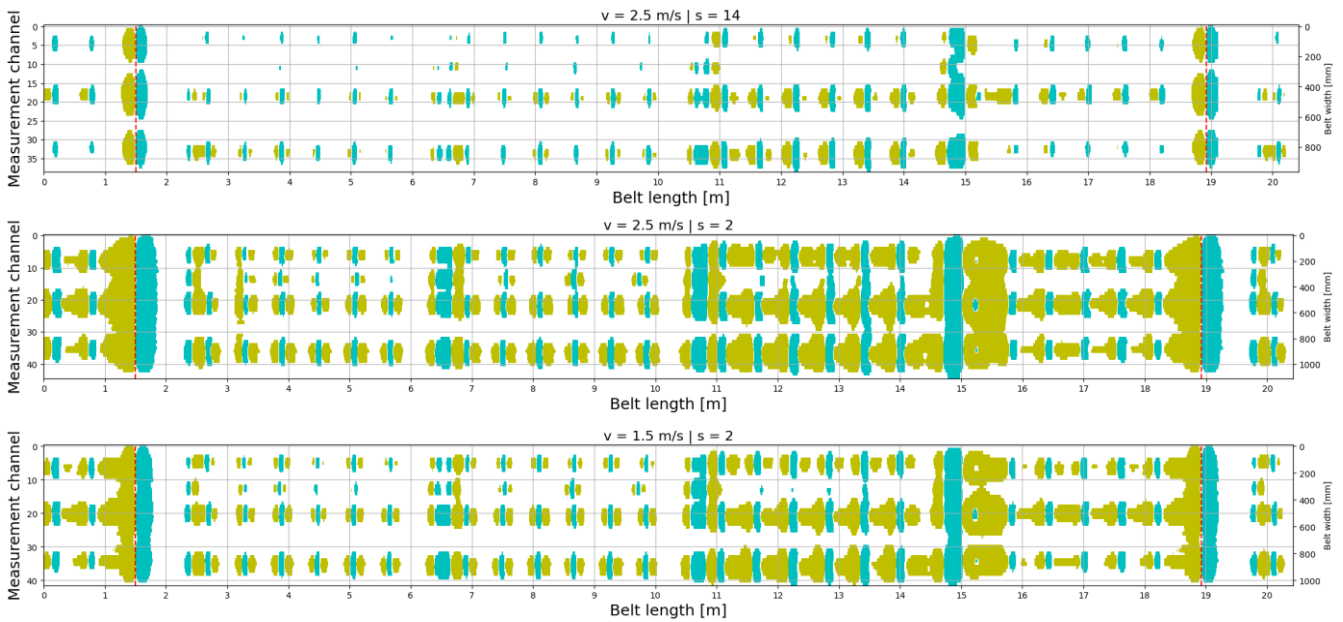


Figure 9. Example visualization of obtained signals for different measurement parameters.

Labels were assigned to the obtained signals based on the type of damage they correspond to. Signals merging with each other were not taken into account. For each set of measurement parameters, four complete measuring loops were recorded. Each area (with the same cord diameter) contained a minimum of three failures of the same type (3 failures of type U1, U2, U3, 3 failures of type B1, B2, B3, and 6 failures of type U50). The average signal magnitude for a given damage was determined from the obtained signals (usually 12 signals), and this value was considered in further analysis.

5. ANALYSIS OF OBTAINED MEASUREMENT RESULTS

Finally, each of the failures was identified and parameterized by measuring key parameters - width, length, and surface area, creating a database for further analysis. Some of the damage signals were not considered due to the merging of signals from one damage with another, making it impossible to separate the signals (e.g., for a signal with parameters $v = 2,5 \frac{m}{s}, s = 2$ only a few failures generated a separable signal). In the end, a total of 8092 damage signals were determined, each described by the parameters of length, width, and surface area (example in Figure 10).

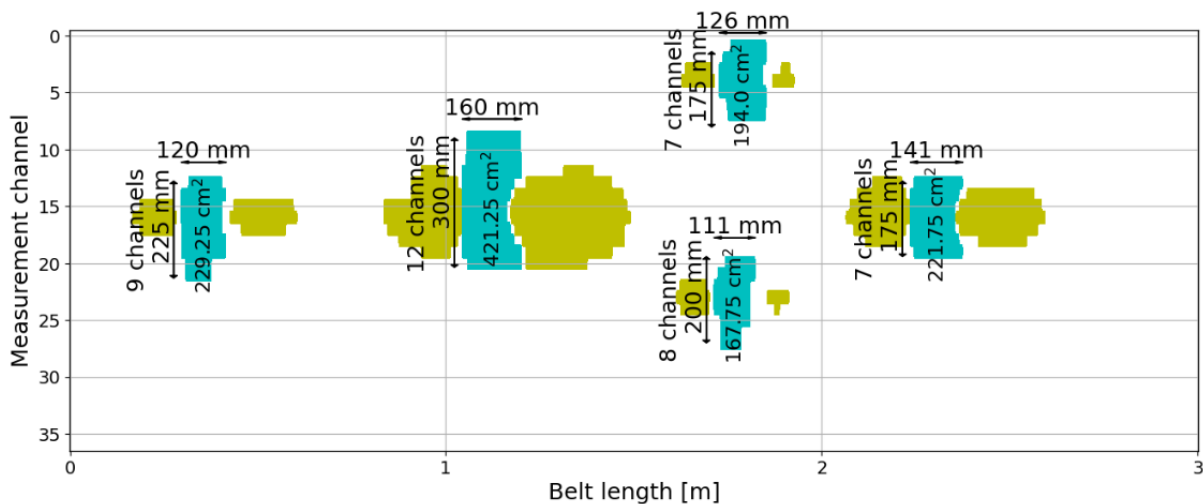


Figure 10. Damage signal parameters.

The database prepared for analysis contains 9 columns:
 v – conveyor belt operating speed during the study [m/s],
 s – sensitivity threshold of the measurement system,
 phi – cord diameter [mm],
 typ – type of damage (see Table 1),
 w – actual width of the damage [mm],
 l – the actual length of the damage [mm],
 a – actual surface area of the damage [cm²],
 anc – the average number of channels occupied by the damage signal,
 aw – average width of the signal [mm].

Data analysis began with measuring the correlation between damage parameters, measurement settings, and measured signal quantities. Figure 11 presents the table of Pearson linear correlation coefficients calculated between each pair of variables. The value of the linear correlation coefficient ranges from -1 to +1 and determines the strength of the linear relationship between variables.

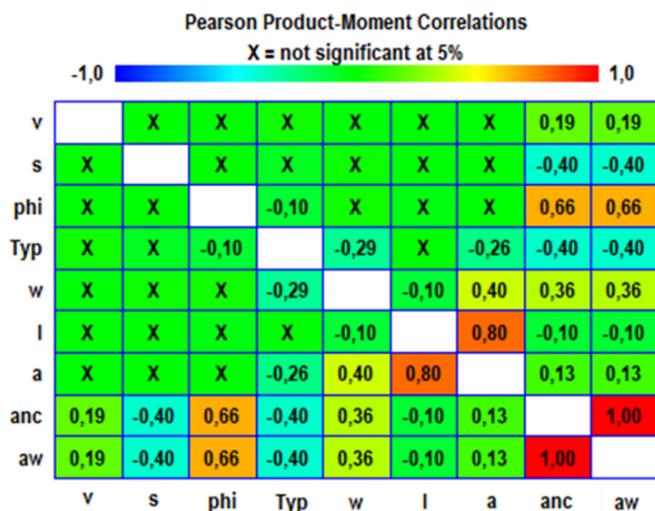


Figure 11. Pearson's linear correlation coefficients for damage parameters, measurement settings, and measured damage signal parameters are presented in the table below. Cells marked with X indicate a non-significant correlation.

The correlation coefficient of 1.00 between aw (average width of the damage) and anc (average number of channels occupied by the damage signal) is due of their linear dependence (equation (3)). Given that the distance between consecutive measuring channels is 25 mm, aw is the product of anc.

The correlation coefficient of 1.00 between aw (average

width of the damage) and anc (average number of channels occupied by the damage signal) is due to their linear dependence (equation 3). Given that the distance between consecutive measuring channels is 25 mm, aw is the product of anc.

$$aw = 25 \cdot anc \quad (3)$$

A high correlation coefficient value of 0.66 was identified between the cord diameter (phi) and the width of the signal anc and aw. A statistically significant correlation value of -0.40 exists for the sensitivity threshold of the system s and the width of the damage signal aw/anc, indicating that an increase in the sensitivity threshold of the system leads to a decrease in the width of the damage signal.

In the next step of the analysis, the distributions of signal widths were examined for failures of different types (Figure 12), obtained for different speeds (Figure 14), for different cord diameters (Figure 16), and for different sensitivity thresholds of the measurement system (Figure 18). The data is presented in box-and-whisker plot format.

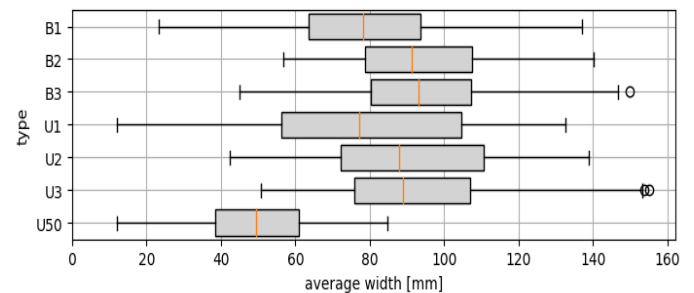


Figure 12. Visualization of damage signal widths depending on the type of damage.

As expected, the width of the signal is the smallest for the U50 signal (simulation of corrosion, loss of 50% of the metallic cross-section of the cord). The signal obtained due to damage to one cord (U1 or B1) is smaller than the signals obtained due to damage to a larger number of adjacent cords. The signal resulting from damage to 3 cords (U3 or B3) is only slightly larger than the signal of damage to two adjacent cords (U2 or B2). However, it should be noted that the transverse resolution of the measuring head is 25 mm, and the cords were embedded in the belt at a distance of 15 mm from each other. This results in a width of 15 mm in the case of damage to one cord, 30 mm in the case of damage to 2 cords, and 45 mm in the case of damage to 3 adjacent cords. Therefore, damage to 2 and 3 cords

corresponds to a real width greater than 1 measuring channel (25 mm) but less than 2 measuring channels (50 mm), which may cause similarities in the widths of obtained signals.

The applied Kruskal-Wallis test checks the null hypothesis that the medians within each of the 7 types of steel cable damage is the same (Table 2). The data from all columns are first combined and ranked from smallest to largest. The average rank is then computed for the data in each column. Since the P-value is less than 0.05, there is a statistically significant difference among the medians at the 95.0% confidence level.

A multiple comparison procedure to determine which means of aw (average width of signal) are significantly different from each other cannot be performed due to the significant differences in standard deviations of aw (average width of signal).

Table 2. Kruskal-Wallis Test for aw (average width of the signal) by type

type	Sample Size	Average Rank
B1	108	308.986
B2	108	424.421
B3	108	434.306
U1	106	315.642
U2	108	398.356
U3	108	413.958
U50	65	89.4615

Test statistic = 160,09 P-Value = 0

Pairwise comparisons between the average ranks of the 7 groups were conducted. Using the Bonferroni procedure, 13 of the comparisons are statistically significant at the 95.0% confidence level.

It's worth noting that the median of the average width for only certain pairs of damage types turned out to be statistically insignificant. These pairs include B1 and U1, B2 and B3, B2 and U2, B2 and U3, B3 and U2, B3 and U3, U1 and U2, U2 and U3. However, it is important to acknowledge that various failures (7), sensitivities (9), speeds (3), and cord diameters (4) were investigated. Field studies are conducted for one combination of parameters since the cord division and belt speed are already chosen, and only a few sensitivities can be tested. Limiting the number of combinations for one cord diameter (7.8) and one sensitivity (12), the image changes somewhat (Figure 13).

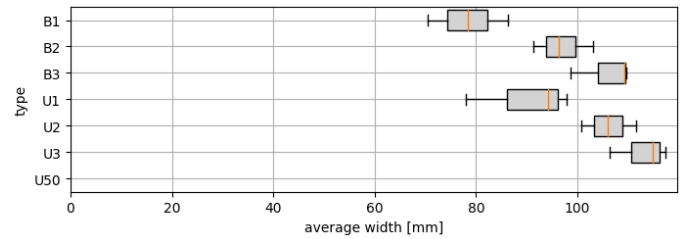


Figure 13. Visualization of the width of damage signals depending on the type of damage for $\phi = 7.8$ mm and $s = 12$.

To assess the impact of belt speed on signal magnitude, comparisons were made across various types of damage (Figure 14).

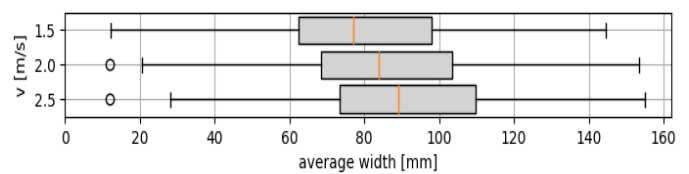


Figure 14. Visualization of the width of damage signals depending on the belt speed during measurement.

The relationship between the width of damage signals and belt speed is evident, showing an increase in average signal width with higher speeds (Pearson's linear correlation coefficient: 0.19).

Table 3. Table of average values of aw (average signal width) according to v (belt speed during measurement) with LSD (Least Significant Difference) intervals at a confidence level of 95.0%.

Table 4. Table of average values of aw (average signal width) according to v (belt speed during measurement) with LSD (Least Significant Difference) intervals at a confidence level of 95.0%.

v	Count	Mean	Std. Error (pooled s)	Lower limit	Upper limit
1.5	232	78.5298	1.71679	76.1505	80.9091
2.0	238	85.461	1.69501	83.1119	87.8101
2.5	241	91.1756	1.68443	88.8412	93.5101
Total	711	85.1364			

Table 3 presents the average value of aw (average signal width) for each belt speed, along with the standard error for each mean, indicating its sampling variability. The standard error is calculated by dividing the pooled standard deviation by the square root of the number of observations at each level. The table also includes intervals around each mean, based on Fisher's least significant difference (LSD) procedure. These

intervals are constructed to overlap 95.0% of the time if two means are the same. In the Multiple Range Tests, these intervals help identify which means are significantly different from others.

Table 5. Multiple Range Tests for aw by v, Method: 95.0 percent LSD.

V [m/s]	Count	Mean	Homogeneous Groups
1.5	232	78.5298	X
2	238	8.,461	X
2.5	241	91.1756	X
Contrast	Sig.	Difference	+/- Limits
1.5 - 2	*	-6.9312	4.72853
1.5 - 2.5	*	-12.6458	4.71398
2 - 2.5	*	-5.7146	4.68361

* denotes a statistically significant difference

Table 5 employs a multiple comparison procedure to identify statistically significant differences among means of

aw (average signal width). The bottom half of the output displays estimated differences between each pair of means, with asterisk denoting significant differences at the 95.0% confidence level. The top section identifies homogenous groups using columns of X's. Within each column, the levels containing X's form a group of means within which there are no statistically significant differences. The method currently being used to discriminate among the means is Fisher's least significant difference (LSD) procedure. With this method, there is a 5.0% risk of calling each pair of means significantly different when the actual difference is zero.

When focusing on one cord diameter ($\phi=7.8$) and one sensitivity, linear regression curves and linear derivatives can be selected (Figure 15)

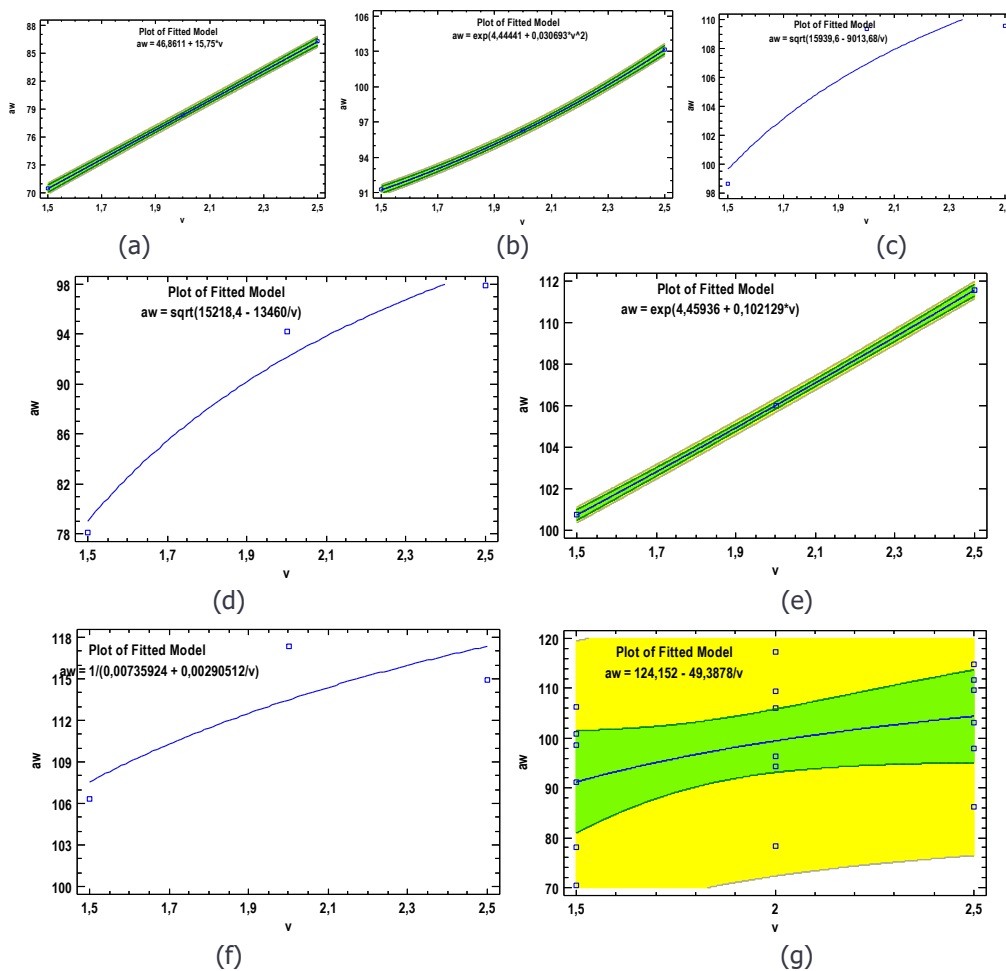


Figure 15. Simple regression of aw versus v for $\phi=7.8$ and $s=12$ for each type of failures: (a) B1, (b) B2, (c) B3, (d) U1, (e) U2, (f) U3, (g) all 6 cable failures on one chart; x axis (v) – velocity [m/s], y axis (aw) – average signal width [mm].

To assess the impact of cord diameter on the mean signal width (aw), a parallel analysis can be performed. It is reasonable to anticipate that both belt speed and the quantity of metal in the cord (its diameter) would positively influence signal strength

and consequently, its width. This expectation is confirmed in Figure 16, where an increase in cord thickness leads to a significant enhancement in mean signal width in both dimensions, with statistical significance.

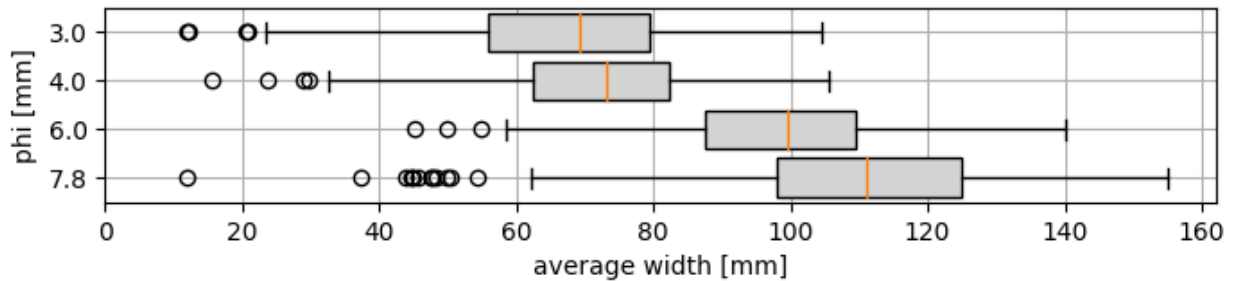


Figure 16. Visualization of signal width concerning cord diameter.

The width of the signal obtained varies depending on the diameter of the cord where the damage was inflicted. The larger the cord diameter, the wider the average signal width of the obtained damage image.

Due to the statistically significant difference among the standard deviations at the 95.0% confidence level, the Kurskal-Wallis test was employed to test the null hypothesis that the medians within each of the four columns is the same. We can find a linear regression model for all data (Figure 17).

Standard Error of Est. = 3392.42
 Mean absolute error = 2554.82
 Durbin-Watson statistic = 0.98603 (P=0.0000)
 Lag 1 residual autocorrelation = 0.506573

The results of the regression analysis present the outcomes of fitting a squared-Y model to describe the relationship between the signal width and the cord diameter. Equation

$$(4) \text{ represents the formula of the fitted model.} \\ aw = \sqrt{-790.087 + 1700.1 \cdot \phi} \quad (4)$$

Since the P-value in the ANOVA analysis is less than 0.05, there is a statistically significant relationship between aw and phi at the 95.0% confidence level.

The R² statistic indicates that the model as fitted explains 46.5224% of the variability in aw after transforming to a reciprocal scale to linearize the model. The correlation coefficient equals 0.682073, indicating a moderately strong relationship between the variables. The standard error of the estimate shows the standard deviation of the residuals to be 3392.42.

Similarly, we can analyze the influence of the selected sensitivity level of the DiagBelt+ device on the average width of the signal indicating failures. Multiple sample comparisons for each set of data for different sensitivity levels can be observed on the box and whiskers chart (Figure 18).

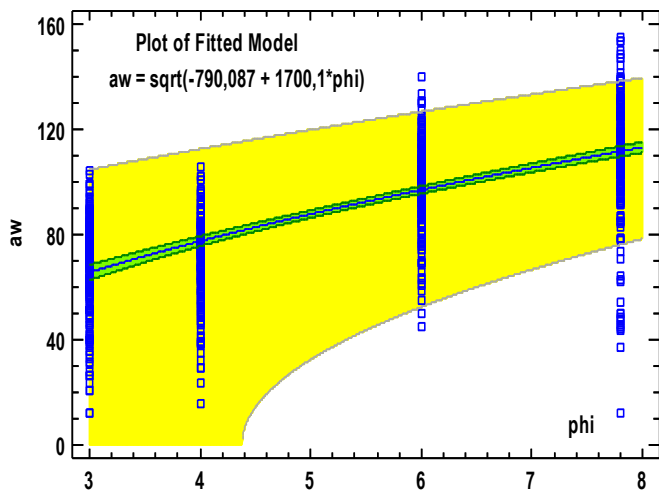


Figure 17. Simple regression model – aw vs. Phi.

Correlation Coefficient = 0.682073
 R² = 46.5224%
 R² (adjusted for d.f.) = 46.447%

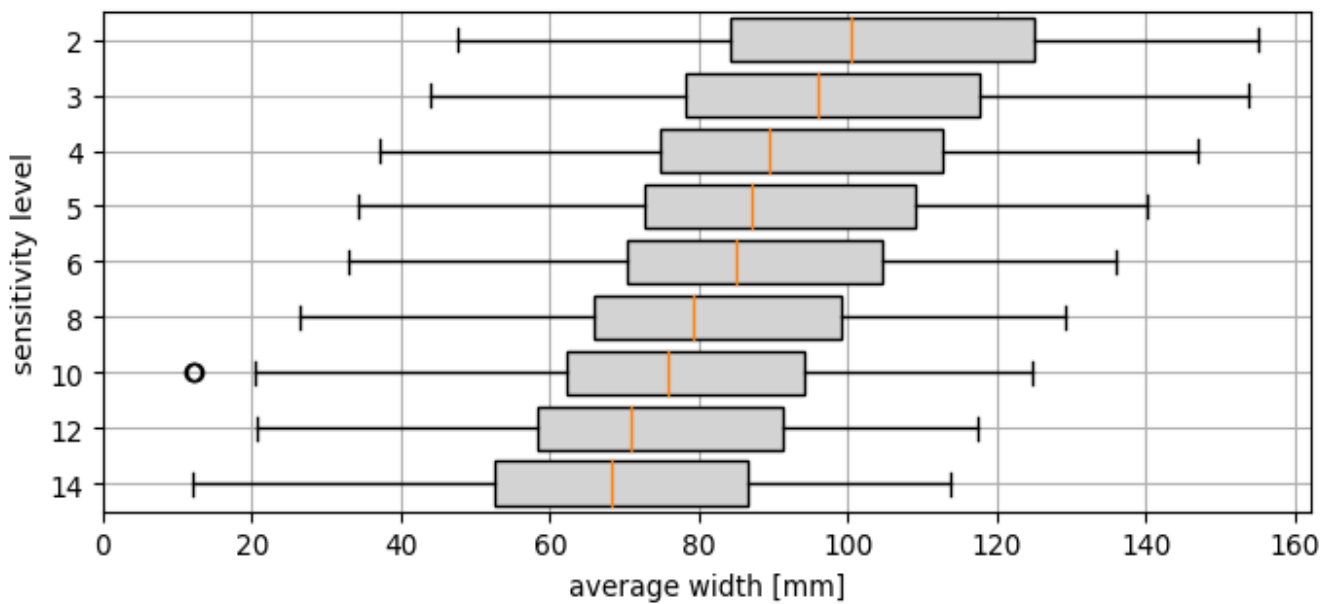


Figure 18. Visualization of signal width for damage depending on the sensitivity threshold of the system.

With the increase in the sensitivity threshold of the system, the average width of the signal decreases. This relationship is also confirmed by the value of the Pearson linear correlation coefficient (-0.40). The table of Pearson linear correlation is a useful tool for assessing the strength of linear relationships between variables, but its limitation is only considering linear relationships. Thanks to axis transformations, it is also possible to explore nonlinear models. For the relationship between aw and s, a Squared-Y logarithmic-X model was selected (Figure 19).

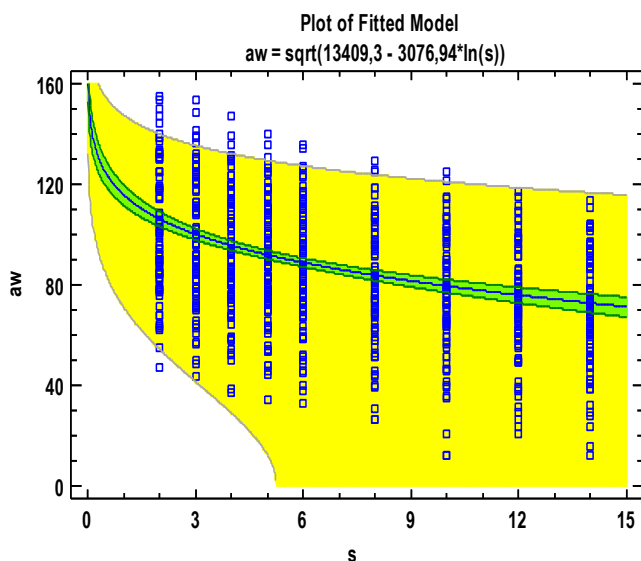


Figure 19. Fitted model for linear regression of aw versus s.

Correlation Coefficient = -0.409038

$R^2 = 16.7312\%$

R^2 (adjusted for d.f.) = 16.6137%

Standard Error of Est. = 4233.16

Mean absolute error = 3476.79

Durbin-Watson statistic = 0.735104 (P=0.0000)

Lag 1 residual autocorrelation = 0.63136

Results of the regression analysis present the outcomes of fitting a Squared-Y logarithmic-X model to describe the relationship between the signal width and the sensitivity threshold. Equation (5) represents the formula of the fitted model.

$$aw = \sqrt{13409.3 - 3076.94 \cdot \ln(s)} \quad (5)$$

Since the P-value in the ANOVA table is less than 0.05, there is a statistically significant relationship between aw and s at the 95.0% confidence level. The R^2 statistic indicates that the model as fitted explains 16.7312% of the variability in aw. The correlation coefficient equals -0.409038, indicating a relatively weak relationship between the variables. The standard error of the estimate shows the standard deviation of the residuals to be 4233.16.

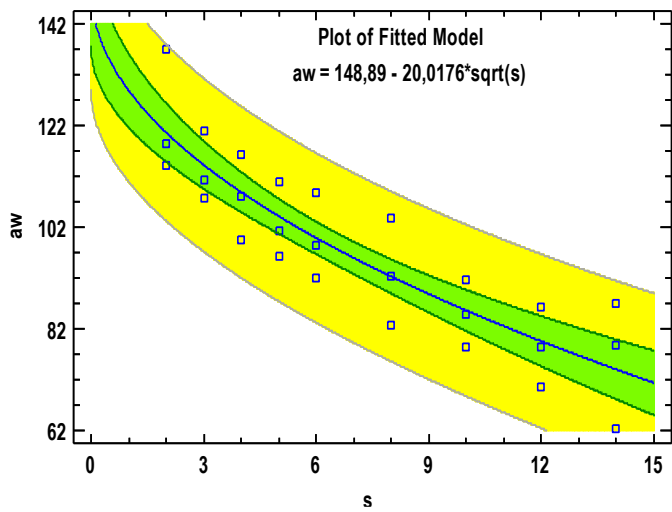


Figure 20. Fitted model for linear regression of aw versus s for cord diameter phi=7.8 mm and damage type="B1".

Correlation Coefficient = -0.891161

$R^2 = 79.4168\%$

R^2 (adjusted for d.f.) = 78.5935%

Standard Error of Est. = 7.9548

Mean absolute error = 6.52263

Durbin-Watson statistic = 0.448064 (P=0.0000)

Lag 1 residual autocorrelation = 0.759711

Results of the regression analysis present the outcomes of fitting a square root-X model to describe the relationship between the signal width and the sensitivity threshold. Equation (6) represents the formula of the fitted model.

$$aw = 148.89 - 20.0176 \cdot \sqrt{s} \quad (6)$$

Since the P-value in the ANOVA table is less than 0.05, there is a statistically significant relationship between aw and s at the 95.0% confidence level. The R^2 statistic indicates that the model as fitted explains 79.4168% of the variability in aw. The correlation coefficient equals -0.891161, indicating a moderately strong relationship between the variables. The standard error of the estimate shows the standard deviation of the residuals to be 7.9548. It is therefore obvious that restriction of number of parameters used can improve R^2 significantly.

3 points on the charts are for different belt speed levels (Figure 21).

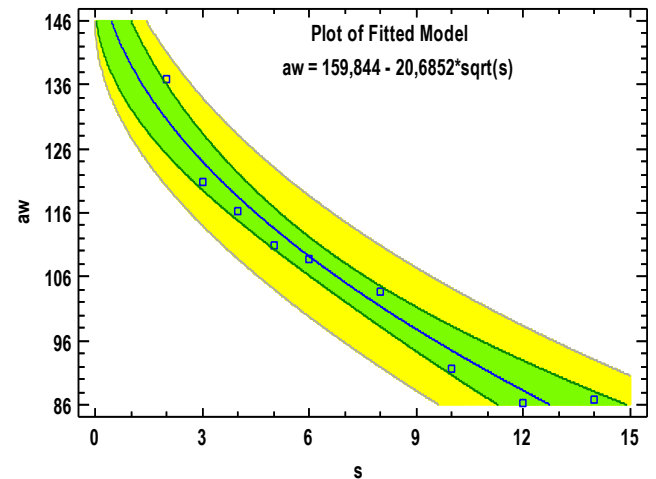


Figure 21. Fitted model for linear regression of aw versus s for cord diameter phi=7.8 mm, damage type="B1" and belt speed v=2.5 m/s.

Correlation Coefficient = -0.977661

$R^2 = 95.5821\%$

R^2 (adjusted for d.f.) = 94.951%

Standard Error of Est. = 3.78755

Mean absolute error = 2.93524

Durbin-Watson statistic = 1.52415 (P=0.1628)

Lag 1 residual autocorrelation = 0.173139

Results of the regression analysis present the outcomes of fitting a square root-X model to describe the relationship between the signal width and the sensitivity threshold. Equation (7) represents the formula of the fitted model.

$$aw = 159.844 - 20.6852 \cdot \sqrt{s} \quad (7)$$

Since the P-value in the ANOVA table is less than 0.05, there is a statistically significant relationship between aw and s at the 95.0% confidence level. The R^2 statistic indicates that the model as fitted explains 95.5821% of the variability in aw. The correlation coefficient equals -0.977661, indicating a relatively strong relationship between the variables. The standard error of the estimate shows the standard deviation of the residuals to be 3.78755.

The mean absolute error (MAE) of 2.93524 is the average value of the residuals. The Durbin-Watson (DW) statistic tests the residuals to determine if there is any significant correlation based on the order in which they occur in your data file. Since the P-value is greater than 0.05, there is no indication of serial autocorrelation in the residuals at the 95.0% confidence level.

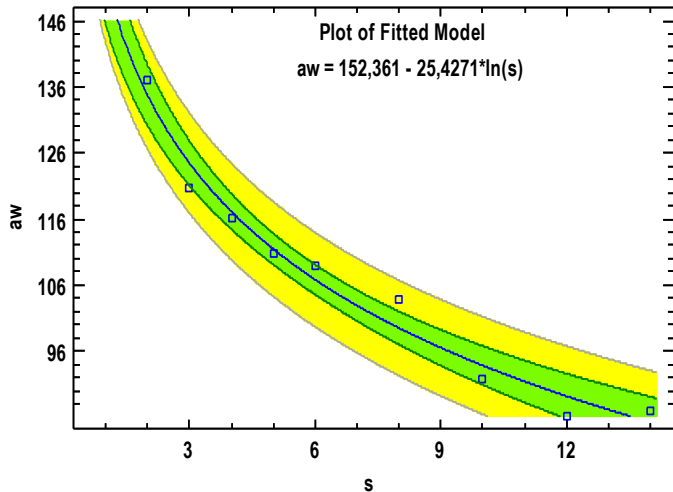


Figure 22. Fitted model for linear regression of aw versus s for cord diameter $\phi=7.8$ mm, damage type="B1" and belt speed $v=2.5$ m/s.

Correlation Coefficient = -0.987302

$R^2 = 97.4766\%$

R^2 (adjusted for d.f.) = 97.1161%

Standard Error of Est. = 2.86249

Mean absolute error = 2.25188

Durbin-Watson statistic = 1.33724 ($P=0.0987$)

Lag 1 residual autocorrelation = 0.135857

Results of the regression analysis present the outcomes of fitting a logarithmic-X model to describe the relationship between the signal width and the sensitivity threshold. Equation

(8) represents the formula of the fitted model.

$$aw = 152.8361 - 25.4271 \cdot \ln(s) \quad (8)$$

Since the P-value in the ANOVA table is less than 0.05, there is a statistically significant relationship between aw and s at the 95,0% confidence level. The R^2 statistic indicates that the model as fitted explains 97,4766% of the variability in aw after transforming to a $Y/(1-Y)$ scale to linearize the model. The correlation coefficient equals -0.987302 , indicating a relatively strong relationship between the variables. The standard error of the estimate shows the standard deviation of the residuals to be 2.86249 .

The mean absolute error (MAE) of 2.25188 is the average value of the residuals. The Durbin-Watson (DW) statistic tests the residuals to determine if there is any significant correlation based on the order in which they occur in your data file. Since the P-value is greater than 0.05, there is no indication of serial autocorrelation in the residuals at the 95.0% confidence level.

6. CONCLUSION

The implementation of the DiagBelt+ system at the Bełchatów Lignite Mine (KWB Bełchatów) brings tangible benefits from both a technical and diagnostic perspectives. This system allows for a more precise assessment of the technical condition of conveyor belts compared to the previously used measure (visual assessment + belt lifespan). Efficiently directing belts for refurbishment based on data from the DiagBelt+ system reduces downtime and contributes to cost savings by eliminating the need to dismantle belts that are still in good technical condition but have been in use for an extended period. Conventional measures, such as total working time, are not ideal for assessing the degree of belt wear. In the study [22], new relative measures were introduced, defined as longitudinal (EX_X) and transverse (EX_Y) extent, to enhance the detection of critical threats. The focus was on the transverse extent, as it plays a crucial role in evaluating tensile strength in the area of damage concentration. This is also essential for proper refurbishment, as significant defects in one section may require additional repairs, necessitating an additional connection at that point. Many algorithms for damage detection and identification have been proposed so far [10, 20, 24, 29, 33, 39, 44, 45]. In this article, we focus on the application of the DiagBelt+ system, which utilizes a magnetic method for identifying failures in the core of conveyor belts. The diagnostics of belts using the DiagBelt+ system allows for identifying the location of damage, and the signal of the damage itself varies depending on the type of damage. However, numerous parameters influence the signal magnitude, and difficulties in labeling signals make it challenging to precisely assess the relationship between signal size and the actual extent of damage. In the analysis of conveyor belts with simulated failures conducted using the DiagBelt+ magnetic system, various factors affecting measurement signals were considered. The research included different types of damage, such as a 50% loss of the metallic cross-section of the cord, cuts in the cords, and the absence of adjacent cords over a short distance (20 mm).

The statistical analyses revealed complex relationships between damage parameters and measurement signals. Independent factors, such as belt speed, cord diameter in the mounted belt, and factors controlled by the operator, like the

sensitivity threshold used, significantly impact the force and measurement signals and the size of their digital image. Some damage groups, such as differences in cord diameter (e.g., 3 mm and 4 mm) or different types of failures (e.g., U1 and U2), form homogeneous damage groups concerning the size of their transverse extent. The absence of statistically significant reasons to reject the hypothesis of the equality of means or medians suggests that the generated signals are very similar. Consequently, the authors plan to utilize artificial intelligence (AI) mechanisms capable of identifying essential features not directly detected by statistical analyses. Currently, research is being conducted on the classification of signals obtained from scanning conveyor belts in the industry and the development of a measure for assessing the technical condition of the belt. This assessment takes into account not only the number of failures per linear meter of the belt (damage density) but also considers the type of each damage. Different types of failures should not be treated equally, as they do not equally reduce the local strength of the belt. Therefore, damage to multiple adjacent cords should be distinguished from damage to one cord. The preparation of a model belt and the conducted studies on it allow for the creation of a database of failures with known parameters, which will be used for training a neural network. Simultaneously, research is also being conducted using artificial intelligence to predict the rate of damage occurrence (deterioration of technical condition measured over time) using data from scanning working belts in real conditions, of various ages, on different conveyors, and transporting different types of materials. The article demonstrates that signal magnitude depends on multiple variables (such as cord diameter, belt speed, and damage type), making it challenging to establish

a multidimensional statistical model. The application of AI technology holds promise for extracting significant patterns and features, significantly aiding in the precise assessment of obtained signals. One of the tasks of the DiagBelt+ system will be predicting the Remaining Useful Life (RUL) of a conveyor belt segment in a loop operating under various conditions. To enhance the accuracy of RUL prediction for belt segments in the loop, the method proposed in [26] can be applied. This involves optimizing the LSTM (Long Short-Term Memory) network through the Harris Hawk optimization algorithm for predicting the RUL of the belt segment. Future perspectives include further research on aligning mathematical models, increasing their accuracy through expanding the database (exploring different sensitivity thresholds and belt speeds), and incorporating results from industrial practice (belts directed for refurbishment have milled covers, enabling the measurement of damage dimensions and linking them to the diagnostic system's obtained image). The overall work may contribute to developing more precise diagnostic tools for conveyor belts, ultimately enhancing the reliability and efficiency of the DiagBelt+ system.

The article provides an evaluation of the relationship between signal magnitude and various parameters, yet a crucial next step may involve conducting statistical analysis focusing on the correlation between signal size and the actual damage size (the ratio of aw to w). Considering nonlinear models accommodating nonlinear dependencies between these variables would be beneficial, as it could help determine the relationship between signal magnitude and the actual extent of damage. Such a model could be valuable in the industry for predicting the actual size of damage based on data collected during diagnostic examinations.

References

1. Andrejiova, M. et al.: Measurement and simulation of impact wear damage to industrial conveyor belts. *Wear*. 368–369, (2016). <https://doi.org/10.1016/j.wear.2016.10.010>.
2. Bajda, M., Hardygóra, M.: Laboratory tests of operational durability and energy-efficiency of conveyor belts. In: *IOP Conference Series: Earth and Environmental Science*. (2019). <https://doi.org/10.1088/1755-1315/261/1/012002>.
3. BeltScan Pty: <https://www.beltscan.com/products/belt-scanner-portable-condition-monitoring.html>.
4. Błażej, R. et al.: Profitability of conveyor belt refurbishment and diagnostics in the light of the circular economy and the full and effective use of resources. *Energies (Basel)*. 15, 20, (2022). <https://doi.org/10.3390/en15207632>.
5. Błażej, R. et al.: The use of magnetic sensors in monitoring the condition of the core in steel cord conveyor belts – Tests of the measuring probe and the design of the DiagBelt system. *Measurement (Lond)*. 123, (2018). <https://doi.org/10.1016/j.measurement.2018.03.051>.

6. Bortnowski, P. et al.: Types and causes of damage to the conveyor belt – Review, classification and mutual relations, (2022). <https://doi.org/10.1016/j.engfailanal.2022.106520>.
7. Bugaric, U. et al.: Lost production costs of the overburden excavation system caused by rubber belt failure. *Eksploracja i Niezawodnosc*. 14, 4, (2012).
8. Che, H. et al.: A reliability model for load-sharing K-out-of-N systems subject to soft and hard failures with dependent workload and shock effects. *Eksploracja i Niezawodnosc*. 22, 2, (2020). <https://doi.org/10.17531/ein.2020.2.8>.
9. Chen, X. et al.: Wear and aging behavior of vulcanized natural rubber nanocomposites under high-speed and high-load sliding wear conditions. *Wear*. 498–499, (2022). <https://doi.org/10.1016/j.wear.2022.204341>.
10. Deng, Y., Li, A.: Measurement-Based Damage Detection for Expansion Joints. In: *Structural Health Monitoring for Suspension Bridges*. (2019). https://doi.org/10.1007/978-981-13-3347-7_3.
11. Doroszuk, B., Król, R.: Analysis of conveyor belt wear caused by material acceleration in transfer stations. *Mining Science*. 26, (2019). <https://doi.org/10.5277/msc192615>.
12. Doroszuk, B., Król, R.: Conveyor belt wear caused by material acceleration in transfer stations. *Mining Science*. 26, (2020). <https://doi.org/10.37190/msc192615>.
13. Fedorko, G. et al.: Failure analysis of textile rubber conveyor belt damaged by dynamic wear. *Eng Fail Anal*. 28, (2013). <https://doi.org/10.1016/j.engfailanal.2012.10.014>.
14. Fedorko, G.: Implementation of Industry 4.0 in the belt conveyor transport. *MATEC Web of Conferences*. 263, (2019). <https://doi.org/10.1051/mateconf/201926301001>.
15. Fedorko, G. et al.: Possibilities of failure analysis for steel cord conveyor belts using knowledge obtained from non-destructive testing of steel ropes. *Eng Fail Anal*. 67, (2016). <https://doi.org/10.1016/j.engfailanal.2016.05.026>.
16. Fourie, J. et al.: Condition Monitoring of Fabric-Reinforced Conveyor Belting Using Digital X-Ray Imaging. *Bulk Solids Handling*. 25, 290–294 (2015).
17. Guo, X. et al.: Belt tear detection for coal mining conveyors. *Micromachines (Basel)*. 13, 3, (2022). <https://doi.org/10.3390/mi13030449>.
18. Guo, X. et al.: Damage Detection for Conveyor Belt Surface Based on Conditional Cycle Generative Adversarial Network. *Sensors*. 22, 9, (2022). <https://doi.org/10.3390/s22093485>.
19. Guo, X. et al.: Machine vision based damage detection for conveyor belt safety using Fusion knowledge distillation. *Alexandria Engineering Journal*. 71, 161–172 (2023). <https://doi.org/10.1016/j.aej.2023.03.034>.
20. Hua, J. et al.: High-resolution damage detection based on local signal difference coefficient model. *Struct Health Monit*. 14, 1, (2015). <https://doi.org/10.1177/1475921714546060>.
21. Ilic, D.: Development of design criteria for reducing wear in iron ore transfer chutes. *Wear*. 434–435, (2019). <https://doi.org/10.1016/j.wear.2019.202986>.
22. Jurdziak, L. et al.: Comparison of different metrics of belt condition used in lignite mines for taking decision about belt segments replacement and refurbishment. Presented at the (2024). https://doi.org/10.1007/978-3-031-44282-7_39.
23. Komander, H. et al.: Assessment methods of conveyor belts impact resistance to the dynamic action of a concentrated load. *Eksploracja i Niezawodnosc*. 16, 4, (2014).
24. Lei, Y. et al.: Structural damage detection with limited input and output measurement signals. *Mech Syst Signal Process*. 28, (2012). <https://doi.org/10.1016/j.ymsp.2011.07.026>.
25. Li, X.-G. et al.: Automatic Defect Detection Method for the Steel Cord Conveyor Belt Based on Its X-Ray Images. In: *2011 International Conference on Control, Automation and Systems Engineering (CASE)*. pp. 1–4 IEEE (2011). <https://doi.org/10.1109/ICCASE.2011.5997624>.
26. Ma, N. et al.: Prediction of the Remaining Useful Life of Supercapacitors at Different Temperatures Based on Improved Long Short-Term Memory. *Energies (Basel)*. 16, 14, 5240 (2023). <https://doi.org/10.3390/en16145240>.
27. Mazurek, P. et al.: Influence of the Size of Damage to the Steel Wire Rope on the Magnetic Signature. *Sensors*. 22, 21, 8162 (2022). <https://doi.org/10.3390/s22218162>.

28. Mendes, D. et al.: Enhanced real-time maintenance management model—a step toward Industry 4.0 through Lean: Conveyor belt operation case study. *Electronics (Basel)*. 12, 18, (2023). <https://doi.org/10.3390/electronics12183872>.
29. Mendler, A. et al.: Sensor placement with optimal damage detectability for statistical damage detection. *Mech Syst Signal Process*. 170, (2022). <https://doi.org/10.1016/j.ymssp.2021.108767>.
30. Mi, J. et al.: Importance measure of probabilistic common cause failures under system hybrid uncertainty based on bayesian network. *Eksploracja i Niezawodnosc*. 22, 1, (2020). <https://doi.org/10.17531/ein.2020.1.13>.
31. Olchówka, D. et al.: Statistical analysis and neural network in detecting steel cord failures in conveyor belts. *Energies (Basel)*. 14, 11, (2021). <https://doi.org/10.3390/en14113081>.
32. Pang, Y.: *Intelligent belt conveyor monitoring and control*. (2005).
33. Radzieński, M. et al.: Improvement of damage detection methods based on experimental modal parameters. *Mech Syst Signal Process*. 25, 6, (2011). <https://doi.org/10.1016/j.ymssp.2011.01.007>.
34. Roskosz, M. et al.: Self Magnetic Flux Leakage as a Diagnostic Signal in the Assessment of Active Stress - Analysis of Influence Factors. *Acta Phys Pol A*. 137, 5, 690–692 (2020). <https://doi.org/10.12693/APhysPolA.137.690>.
35. Roskosz, M. et al.: Use of Different Types of Magnetic Field Sensors in Diagnosing the State of Ferromagnetic Elements Based on Residual Magnetic Field Measurements. *Sensors*. 23, 14, 6365 (2023). <https://doi.org/10.3390/s23146365>.
36. Semrád, K., Draganová, K.: Non-destructive testing of pipe conveyor belts using glass-coated magnetic microwires. *Sustainability (Switzerland)*. 14, 14, (2022). <https://doi.org/10.3390/su14148536>.
37. Walker, P. et al.: Analysis of ore flow through longitudinal belt conveyor transfer point. *Eksploracja i Niezawodnosc*. 22, 3, (2020). <https://doi.org/10.17531/ein.2020.3.17>.
38. Wang, J. et al.: Belt vision localization algorithm based on machine vision and belt conveyor deviation detection. In: 2019 34rd Youth Academic Annual Conference of Chinese Association of Automation (YAC). pp. 269–273 IEEE (2019). <https://doi.org/10.1109/YAC.2019.8787667>.
39. Wang, J., Yang, Q.S.: Sensor selection approach for damage identification based on response sensitivity. *Structural Monitoring and Maintenance*. 4, 1, (2017). <https://doi.org/10.12989/smm.2017.4.1.053>.
40. Webb, C. et al.: Developing and evaluating predictive conveyor belt wear models. *Data-Centric Engineering*. 1, 1–2, (2020). <https://doi.org/10.1017/dce.2020.1>.
41. Witoś, M. et al.: NDE of Mining Ropes and Conveyors Using Magnetic Methods. In: International Symposium on Structural Health Monitoring and Nondestructive Testing 4-5 Oct 2018, Saarbrücken – Germany (SHM-NDT 2018) | Vol. 23(12). , Saarbrücken – German (2018).
42. Xie, L. et al.: Wear process during granular flow transportation in conveyor transfer. *Powder Technol*. 288, (2016). <https://doi.org/10.1016/j.powtec.2015.10.043>.
43. Yang, R. et al.: Infrared spectrum analysis method for detection and early warning of longitudinal tear of mine conveyor belt. *Measurement (Lond)*. 165, (2020). <https://doi.org/10.1016/j.measurement.2020.107856>.
44. Yu, J., Zhang, H.: A suspended FBG damage detection sensor based on magnetic drive. *Measurement (Lond)*. 189, (2022). <https://doi.org/10.1016/j.measurement.2021.110499>.
45. Ziehl, P., ElBatanouny, M.: Acoustic emission monitoring for corrosion damage detection and classification. In: *Corrosion of Steel in Concrete Structures*. (2023). <https://doi.org/10.1016/B978-0-12-821840-2.00009-2>.